Astron. Nachr. / AN **332**, No. 9/10, 859 – 865 (2011) / **DOI** 10.1002/asna.201111616

# Spot activity of II Peg[⋆]

**T. Hackman[1,2,⋆⋆], M.J. Mantere[1], L. Jetsu[1], I. Ilyin[4], P. Kajatkari[1], O. Kochukhov[5], J. Lehtinen[1], M. Lindborg[1,3], N. Piskunov[5],** and **I. Tuominen[1,6]**

[1] Department of Physics, P.O. Box 64, FI-00014 University of Helsinki, Finland
[2] Finnish Centre for Astronomy with ESO, University of Turku, Väisäläntie 20, FI-21500 Piikkiö, Finland
[3] Nordic Optical Telescope, 38700 Santa Cruz de la Palma, Spain
[4] Leibniz-Institut für Astrophysik Potsdam, An der Sternwarte 16, D-14882 Potsdam, Germany
[5] Department of Physics and Astronomy, Uppsala University, Box 516, SE-751 20 Uppsala, Sweden
[6] Deceased

Received 2011 Sep 20, accepted 2011 Oct 6
Published online 2011 Dec 12

**Key words** binaries: spectroscopic – stars: activity – stars: individual (II Peg) – starspots – techniques: spectroscopic

We have studied the long-term spot activity of the RS CVn star II Peg by means of Doppler imaging based on spectroscopy and time series analysis of photometry. We present 28 Doppler imaging temperature maps spanning the years 1994–2010, of which 14 were calculated for the present study. The longitudinal spot distribution, derived from the surface temperature maps, is compared with epochs of the light curve minima, derived from photometric observations. We detect a longitudinal drift in the major spot structure during 1995–2003. After this there is a clear decrease in the activity level and no clear drift can be seen. We conclude that the variations could be caused by a cyclic behaviour of the underlying magnetic dynamo.



## 1 Introduction

II Peg is a very active rapidly rotating RS CVn binary, which has been extensively studied with a wide range of instruments, wavelengths and methods. II Peg exhibits several signs of magnetic activity. It is the brightest X-ray source within 50 pc (Makarov 2003) and has displayed one of the highest spot-related photometric amplitudes of late-type stars (Doyle et al. 1989). The star was classified as an RS CVn binary by Rucinski (1977), Vogt (1979), and Bopp & Noah (1980). Several subsequent studies on the stellar parameters of the object have been conducted (e.g. Berdyugina et al. 1998a). We can conclude that II Peg is a one-line spectroscopic binary of spectral class K2 IV with a rotation period of $P_{\rm rot} \approx 6\overset{\rm d}{.}72$ and a rotation velocity of $v \sin i \approx 22.6\,{\rm km\,s^{-1}}$.

The high projected rotation velocity of II Peg makes it a suitable target for Doppler imaging, a technique where the surface is mapped using high-resolution spectroscopic observations. The technique is based on the fact that spots on the surface will introduce distortions in the spectral lines. The surface temperature (or element abundance) distribution can thus be reconstructed by using a series of spectra from different rotational phases (cf. Piskunov 1991).

II Peg has been the focus of several long-term studies based on photometry or spectroscopy. These studies include the detection of activity cycles from photometry (e.g. Henry et al. 1995; Rodonò et al. 2000) and regular switching between two active longitudes, i.e. “flip-flops” (Berdyugina & Tuominen 1998; Berdyugina et al. 1999).

II Peg is included in the long-term observational programmes carried out with the SOFIN high-resolution échelle spectrograph at the 2.56 m Nordic Optical Telescope since 1994. Based on these observations, an extensive time series of Doppler images has been published (Berdyugina et al. 1998b, 1999; Lindborg et al. 2011, hereafter Paper I; Hackman et al. 2011, hereafter Paper II). Since 2004 spectropolarimetric Stokes $I$ and $V$ observations have been collected with SOFIN at NOT. These observations have been used for Zeeman-Doppler imaging by Carroll et al. (2009) and Kochukhov et al. (2009).

Our aim is to study the long-term magnetic activity of II Peg, in particular changes related to a possible stellar cycle. This is done by combining the results from two different techniques. We use the epochs and rotation phases of the photometric minima derived by time series analysis. The high-resolution spectroscopic observations are used for calculating seasonal Doppler imaging temperature maps. In order to study the long-term spot activity more accurately we compile a set of 28 Doppler images derived with consistent parameters.

⋆ Based on observations made with the Nordic Optical Telescope, operated on the island of La Palma jointly by Denmark, Finland, Iceland, Norway, and Sweden, in the Spanish Observatorio del Roque de los Muchachos of the Instituto de Astrofisica de Canarias.

⋆⋆ Corresponding author: Thomas.Hackman@helsinki.fi

**Table 1** Summary of observations with NOT: data set, HJD of first ($t_{\min}$) and last ($t_{\max}$) observation, mean signal-to-noise ratio (S/N), number of observed phases ($n_\phi$), and deviation ($d$) of the Doppler imaging solution.

| Data Set | $t_{\min}$ | $t_{\max}$ | S/N | $n_\phi$ | $d$ |
|---|---|---|---|---|---|
| Aug 94 | 2449578.7 | 2449587.7 | 325 | 10 | 0.00529 |
| Jul 95 | 2449910.7 | 2449921.6 | 303 | 11 | 0.00517 |
| Jul 96 | 2450293.7 | 2450299.7 | 251 | 6 | 0.00470 |
| Oct 96 | 2450381.4 | 2450388.4 | 238 | 9 | 0.00544 |
| Jun 97 | 2450617.7 | 2450627.7 | 265 | 11 | 0.00476 |
| Aug 97 | 2450676.7 | 2450683.8 | 191 | 8 | 0.00580 |
| Dec 97 | 2450794.4 | 2450807.4 | 162 | 12 | 0.00746 |
| Jul 98 | 2450997.7 | 2451010.7 | 209 | 13 | 0.00670 |
| Oct 98 | 2451088.4 | 2451094.5 | 240 | 7 | 0.00492 |
| Nov 98 | 2451121.5 | 2451127.5 | 177 | 7 | 0.00615 |
| Jul 99 | 2451383.7 | 2451394.7 | 212 | 12 | 0.00591 |
| Sep 99 | 2451443.5 | 2451449.6 | 186 | 7 | 0.00532 |
| Oct 99 | 2451471.6 | 2451505.3 | 218 | 5 | 0.00452 |
| Aug 01 | 2452120.6 | 2452130.6 | 192 | 10 | 0.00539 |
| Aug 02 | 2452507.6 | 2452518.6 | 189 | 10 | 0.00582 |
| Nov 02 | 2452588.4 | 2452600.5 | 230 | 7 | 0.00568 |
| Aug 04 | 2453216.6 | 2453228.6 | 244 | 8 | 0.00570 |
| Dec 04 | 2453370.4 | 2453372.4 | 196 | 3 | 0.00619 |
| Jul 05 | 2453567.7 | 2453575.6 | 218 | 7 | 0.00594 |
| Nov 05 | 2453685.5 | 2453695.5 | 197 | 5 | 0.00673 |
| Sep 06 | 2453978.5 | 2453992.7 | 259 | 11 | 0.00610 |
| Dec 06 | 2454071.5 | 2454078.4 | 166 | 7 | 0.00666 |
| Jul 07 | 2454300.7 | 2454309.7 | 264 | 10 | 0.00584 |
| Nov 07 | 2454427.4 | 2454437.4 | 238 | 7 | 0.00619 |
| Sep 08 | 2454717.6 | 2454723.5 | 304 | 4 | 0.00537 |
| Dec 08 | 2454809.4 | 2454815.5 | 263 | 6 | 0.00719 |
| Aug 09 | 2455069.7 | 2455081.7 | 291 | 12 | 0.00682 |
| Dec 09 | 2455193.4 | 2455201.4 | 283 | 8 | 0.00602 |

## 2 Observations

The data for our long-term analysis of II Peg consist of high resolution spectroscopy and a contemporary sequence of $V$-band photometry. The spectroscopic observations were collected with the SOFIN high-resolution échelle spectrograph mounted on the 2.56 m Nordic Optical Telescope. The spectral resolution was $R \approx 70\,000$ and the signal-to-noise ratio usually $\mathrm{S/N} \sim 200$–300. The data were collected during 1994–2010 and each set usually contained $\sim$10 spectra. The spectra were reduced using the the 4A software system (Ilyin 2000). A summary of the data is displayed in Table 1. More detailed descriptions and plots of the data are available in our previous papers (Paper I; Paper II). The observed spectral regions were different for the years 1994–2002 and 2004–2010. The ephemeris used to calculate the rotation phases was that of the orbital period derived by Berdyugina et al. (1998a):

$$T_{\mathrm{conj}} = 2449582.9268 + 6.724333 \times E. \quad (1)$$

The data used for time series analysis were collected with the T3 0.4 APT at Fairborn Observatory (Arizona, USA). These data are described in the study by Jetsu et al. (2011). Most of the same data were also used by Roettenbacher et al. (2011).

## 3 Analysis

Our analysis is based on two methods: The Continuous Period Search method and Doppler imaging. As our results show, it is very important to combine these methods. Doppler imaging will only provide very short snapshots of the target, while, on the other hand, photometry enables a more continuous monitoring but provides much less information than Doppler imaging.

### 3.1 The Continuous Period Search method

The Continuous Period Search method (hereafter CPS) is a newly developed time series analysis code especially intended for analysing stellar spot activity. CPS is based on the Three Stage Period Analysis (TSPA) formulated by Jetsu & Pelt (1999), with three important new features:

1. The time series analysis is applied on the data with a sliding window, thus increasing the time resolution.
2. The Bayesian information criterion is used for selecting the correct order for the model.
3. An estimate of the time scale for significant changes in the light curve is retrieved.

The CPS model consists of a $K$th order Fourier series

$$\hat{y}(t_i) = M + \sum_{k=1}^{K} [B_k \cos(k 2\pi f t_i) + C_k \sin(k 2\pi f t_i)], \quad (2)$$

where the $2K+2$ free parameters are the mean $M$, the individual amplitudes $B_k$ and $C_k$, and the frequency $f$. The search for the best parameter values is done in two steps. In the *grid search* a dense grid of frequencies is tested one by one. The best frequency with its corresponding amplitudes $B_k$ and $C_k$ are then used as a starting point for the *refined search*, which is a standard nonlinear Marquardt iteration. The optimal order $K$ for the model is chosen using the Bayesian information criterion (Stoica & Selén 2004).

The model is applied to the data using a window of length $\Delta T$. Instead of dividing the data into separate sets, the CPS is based on a sliding window. This means that for each new data point, a new model can be applied. The tested data sets are thereby overlapping, and instead of discrete snapshots of the data, we can study continuous changes of all model parameters. A more complete description of the CPS method is presented by Lehtinen et al. (2011).

With the CPS method one can retrieve the light curve mean ($M$), amplitude ($A$), photometric period ($P_{\mathrm{phot}}$) and epochs of the primary and secondary minima ($t_{\mathrm{min},1}$ and $t_{\mathrm{min},2}$) as functions of time. For this study we focused on the photometric minima, which could indicate the existence of persistent active longitudes. The photometric minima, mean magnitudes and light curve amplitudes for II Peg during the years 1994–2010 were retrieved using the CPS method with

 

**Table 2** Adopted stellar parameters: gravity, inclination angle, rotation velocity, rotation period, metallicity, macroturbulence, and microturbulence.

| Stellar Parameter | Value |
|---|---|
| $\log g$ | 3.5 |
| $i$ | 60° |
| $v \sin i$ | 22.6 km s$^{-1}$ |
| $P_{\rm rot}$ | $6\overset{\rm d}{.}724333$ |
| $\log[{\rm M/H}]$ | $-0.25$ |
| $\zeta_{\rm t}$ | 3.5 km s$^{-1}$ |
| $\xi_{\rm t}$ | 1.8 km s$^{-1}$ |

a window of $\Delta T = 30$ d (approx. 4 rotations). The full analysis as well as the numerical results are given in the paper by Jetsu et al. (2011).

### 3.2 Doppler imaging

We used the Doppler imaging technique developed by Piskunov and collaborators to calculate temperature maps for II Peg. The inversion technique uses a pre-calculated table of local line profiles and is based on Tikhonov regularization (Piskunov 1991; Hackman et al. 2001; Paper I).

The line profiles were calculated using MARCS model atmospheres (Gustafsson et al. 2008) with gravity $\log g = 3.5$, metallicity $\log[{\rm M/H}] = -0.25$ and effective temperatures $T_{\rm eff}$ ranging from 3200 K to 6000 K.

It should be pointed out that an exact determination of the stellar parameters was not the aim of the analysis. For example, the choice of microturbulence or element abundances will affect the mean effective temperature of the solution. We used the stellar parameters suggested by Ottmann et al. (1998) as a starting point, meaning that the parameters were optimized for a solution with a mean effective temperature of $T_{\rm eff} \approx 4700$ K. This means that the stellar parameters differ from the ones used in Paper I. The adopted stellar parameters are listed Table 2. More details on the the choice of stellar and spectral parameters are given in Paper II.

All Doppler images were calculated with a regularization parameter of $\Lambda = 1 \times 10^{-9}$ and a grid of $80 \times 40$ surface elements. For a perfect solution the deviation between the observations and the calculated line profiles should correspond to the inverse of the observational $S/N$-value. In practice, systematic errors in the model and observations will make this level hard to achieve. The deviations for each Doppler image are listed in Table 1.

The Doppler imaging maps from 1994–2002 (Fig. 1) were calculated using the spectral regions 6172.5–6174.1 Å, 6174.7–6177.9 Å, and 6179.5–6181 Å. These regions contain the lines Fe I 6173.34 Å, Ni I 6175.36 Å, Ni I 6176.81 Å, Ni I 6177.26 Å, and Fe I 6180.20 Å. For the years 2004–2010 the observations were made in different spectral regions. We then used the regions 5392.3–5395.1 Å, 5524.7–5527.3 Å, and 5633.2–5634.6 Å, containing the lines Fe I 5393.17 Å, Mn I 5394.68 Å, Fe II 5525.12 Å, Fe I 5525.48 Å, Fe I 5525.54 Å, Sc II 5526.79 Å, and Fe I 5633.95 Å.

The Doppler imaging maps are displayed in Fig. 1. The images of 2002–2010 are the same as presented in Paper II. In order to be able to make a more reliable comparison for the whole span of the observations, we recalculated the images of 1994–2001 using the same stellar parameters as in Paper II.

## 4 Results

The main difference between the recalculated images for 1994–2002 and the old ones (Paper I) is a systematic shift in the mean effective temperature. The older images were generally ∼100 K cooler. This is a natural result of the fact that different stellar parameters were used. Comparing the recalculated images from 1994–2002 with the ones from 2004–2010 we again note a systematic difference of ∼50 K in the level of the mean temperatures (Fig. 4). This could be an artifact caused by the use of different wavelength regions, but may also reflect changes in the activity level.

To study the evolution of the spot activity we calculated the mean temperature along both longitudes (or phases) and latitudes. The longitudinal averages can be used to study the spot distribution over rotational phase (Fig. 2). In this plot we also include the photometric minima folded by the orbital period (Eq. (1)). The latitudinal averages (Fig. 3) can be regarded as an analogue to the solar butterfly diagram.

All images contain features which may be artifacts typical for Doppler imaging, e.g. alternating cool and hot regions (Hackman et al. 2001). Particular caution should be applied when interpreting images based on only 3–6 observed phases i.e. the images from July 1996, October 1999, December 2004, November 2005, September 2008 and December 2008. A criterion for the reliability of a Doppler image is that the main cool spot concentration is centered on the same rotation phase as the photometric minimum. Here one should, of course, take into account that the minimum may be a result of the combined effect of several spots. Nevertheless, the comparison of the spot distribution and photometric minima in Fig. 2 shows that the main spot region may have been missed in the Doppler images from December 2004 and November 2005 because of insufficient phase coverage.

The longitudinal averages, combined with the photometric minima, reveal a drift of the main active region occurring during the years 1995–2003 (Fig. 2). This drift is not present anymore during 2004–2010. Instead the spot distribution is more random, although there is a clear tendency of the main spots to be centered in the phase range 0.7–1.0. This tendency is again supported by the distribution of the phases of the photometric minima. We do not see any signs of flip-flops occurring during 1994–2010. The same result was also obtained in our earlier studies (Papers I and II).

The latitudinal distribution (Fig. 3) does not reveal any clear trends. In general, the main spot regions are centered

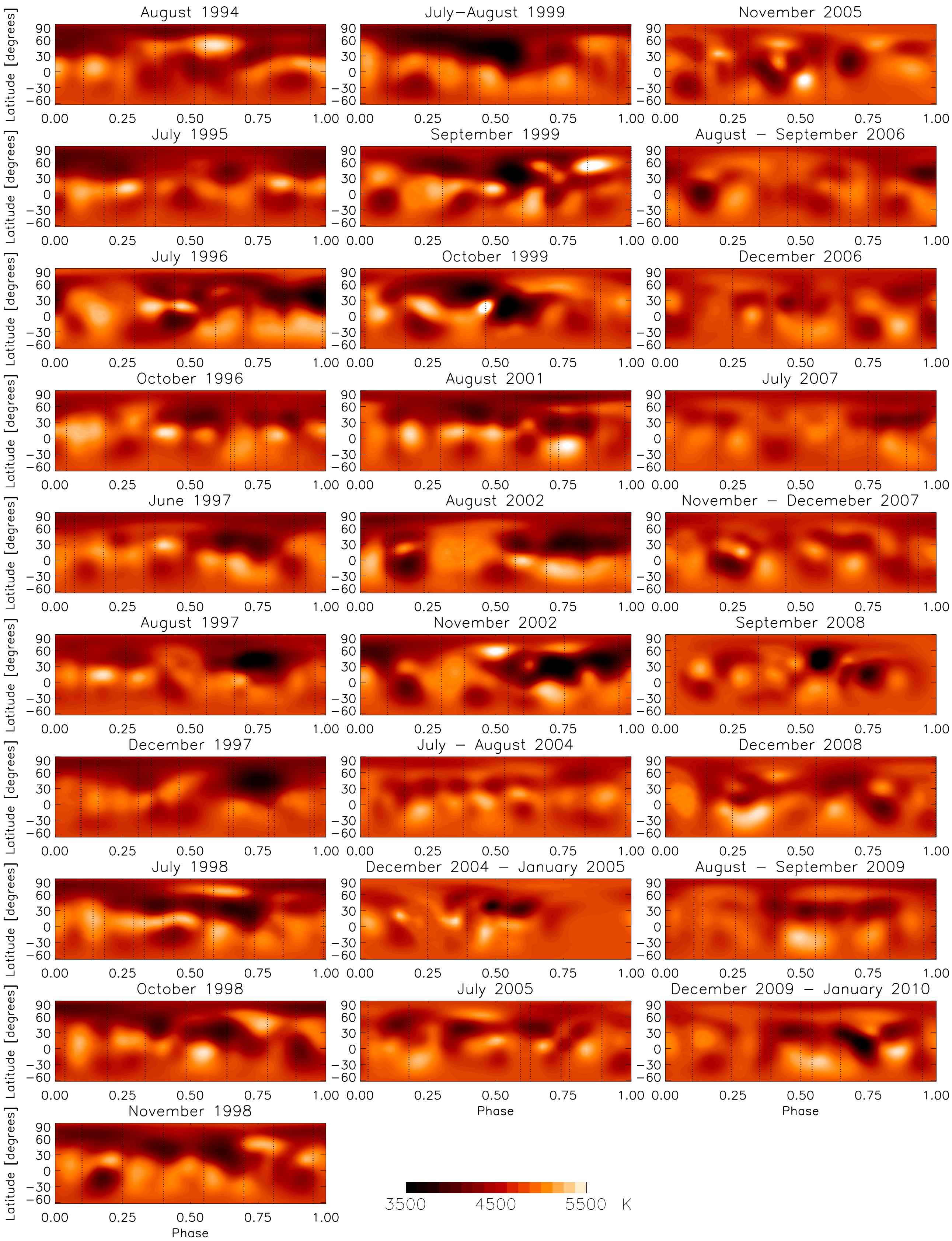


**Fig. 1** (online colour at: www.an-journal.org) Doppler images of II Peg from the years 1994–2010. The dashed vertical lines mark the phases of the observations. The images from 2002–2010 are from Hackman et al. (2011).

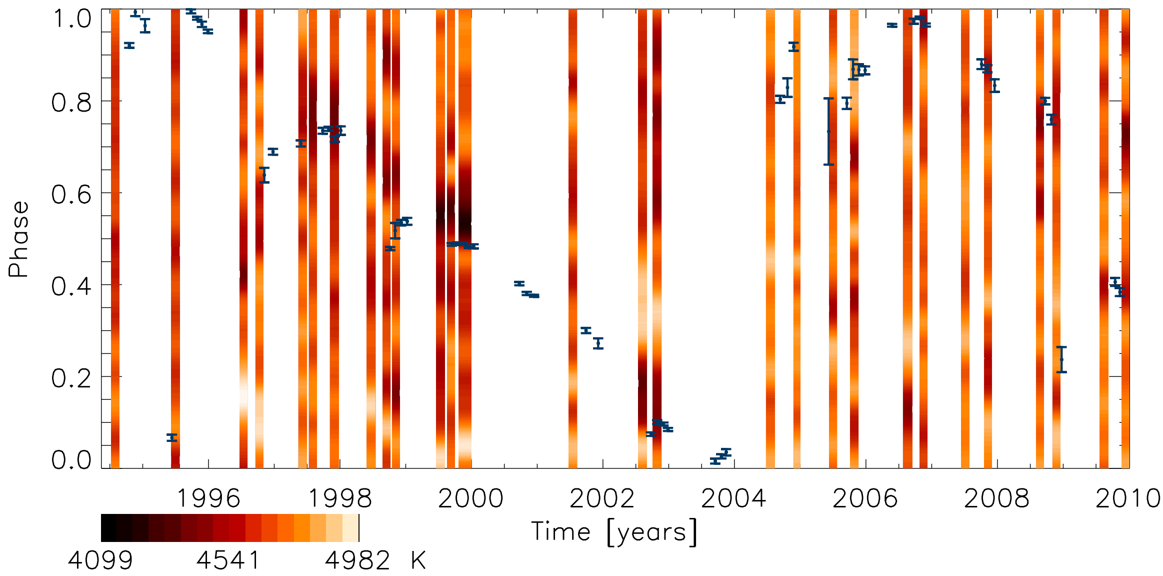


**Fig. 2** (online colour at: www.an-journal.org) Average surface temperature, calculated from the temperature maps over the whole latitude range, as a function of phase. Each stripe represents one Doppler image, but the width (in time) is slightly increased in order for more clear display. The points with error bars mark the photometric minima.

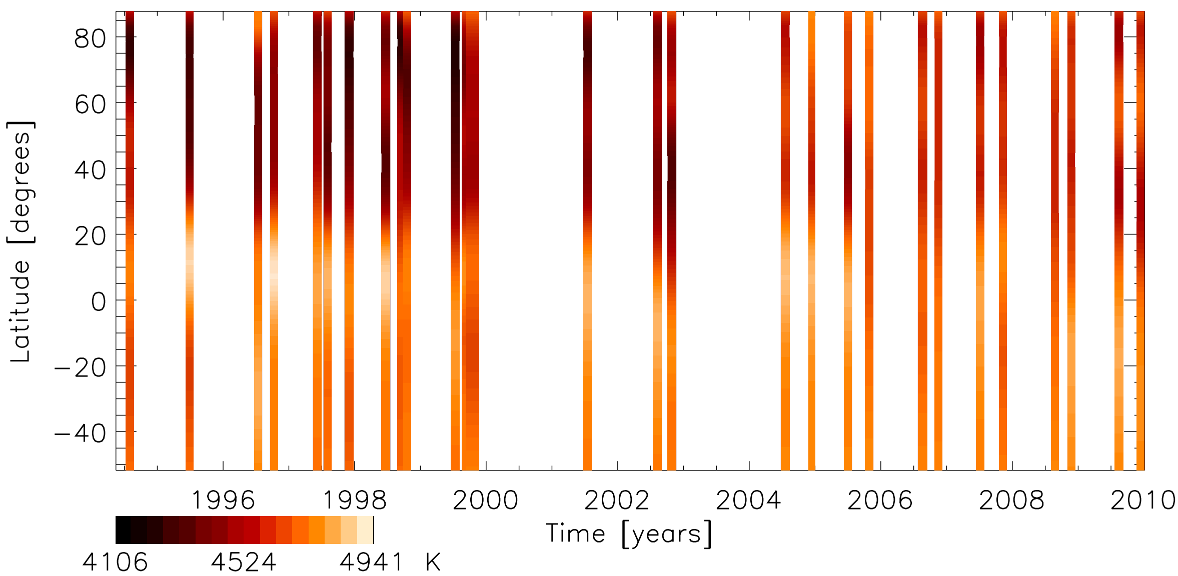


**Fig. 3** (online colour at: www.an-journal.org) Average surface temperature, calculated from the surface temperature maps over the whole longitude range, as a function of latitude. Each stripe represents one Doppler image, but the width (in time) is slightly increased in order for more clear display.

at latitudes 40–70°, i.e. higher than in the case of the Sun. However, a clear tendency for both the Doppler images, and the latitudinal and longitudinal means, is the generally higher level of spot activity during 1994–2002 than 2004–2010. To quantify the activity level we estimated the amount of stellar surface covered by spots. As noted before, the use of different wavelength regions might have introduced some systematic bias into the mean effective temperature $T_{\rm mean}$ of the Doppler imaging solutions. Therefore we define the spot coverage as the percentage of the surface with an effective temperature below $T_{\rm mean} - 300$ K. As should be, we can see that there is a negative correlation between the mean temperature and the spot coverage (Fig. 4). As an independent check, we also plot the results from the CPS analysis of photometry carried out by Jetsu et al. (2011). The mean differential magnitude of II Peg is in fact generally higher and the photometric amplitude lower after the year 2002.

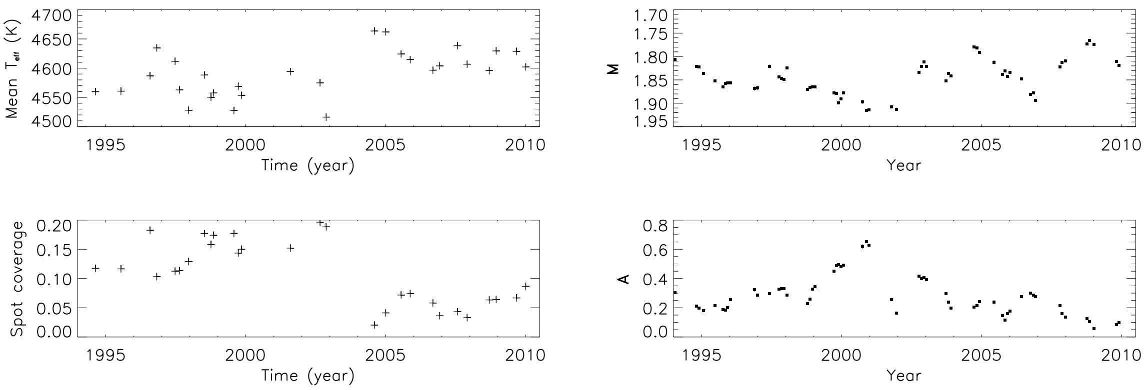


**Fig. 4** The spot activity level quantified by the mean effective temperature (*upper left*), spot coverage (*lower left*), mean differential magnitude (*upper right*), and light curve amplitude (*lower right*).

## 5 Conclusions

We have monitored the spot activity of II Peg during 1994–2010 utilizing high-resolution spectroscopy and photometry. We see no evidence of a regular flip-flop behaviour. Instead of two active longitudes changing strength periodically, we see one dominant active longitude, which during 1995–2003 is rotating faster (i.e. with a shorter period) than the stellar surface, presumably synchronized with the orbital period of the binary. This could be explained by an azimuthal dynamo wave. During the years 2004–2010 there is, however, no clear trace of such a wave. This could be connected to the low activity level during this period.

A problem in our analysis is that the spectroscopic setup was changed between the 2002 and 2004 observations, i.e. during the same period as there were significant changes in the activity level. This raises the question whether the difference in the observed mean temperature and spot coverage could be caused by the usage of different spectral regions. However, the photometric observations also support the changes in the activity level.

Cool spots on late-type stars are generally interpreted as a result of magnetic fields penetrating the surface and inhibiting convection, i.e. the analogue to the solar case. In a recent study Käpylä et al. (2011) showed that both cool and hot spots can be generated without magnetic fields. In the case of II Peg the presence of large magnetic structures on the surface have been confirmed by Zeeman-Doppler imaging (Carroll et al. 2009; Kochukhov et al. 2009). Although the relation between the magnetic fields and the cool spots is not yet clear, we still interpret the spot activity as a result of a magnetic dynamo operating in the convective zone.

The observed drift of the spot structure in II Peg is best explained by an azimuthal dynamo wave. Such waves are expected to occur in rapidly rotating late-type stars (e.g. Krause & Rädler 1980; Tuominen et al. 2002). The fact that the wave disappears can be explained by evolution connected to a stellar cycle. Another explanation for the drift could be provided by a not yet completely synchronized rotation profile of the star to the orbital period of the binary. However, the fact that the drift is observed to disappear proves this scenario very unlikely. Yet an alternative explanation for the spot drift would be surface differential rotation, which would mean that spots at different latitudes would follow different rotation velocities.

Roettenbacher et al. (2011) and Siwak et al. (2010) found proof of differential rotation by tracing the movements of individual spots using ground based and satellite based photometry. However, we do not see any tendency in the spot latitude which should be present, if surface differential rotation would cause the drift. Furthermore, from the Doppler images it is clear that the spot configuration changes on a time scale of weeks or months rather than years. Thus the drifting active region does not represent exactly the same spot structure, but rather a region which is fed by an underlying magnetic structure.

*Acknowledgements.* This work was supported by the "Active Suns" research project at the University of Helsinki (TH), the Academy of Finland projects 218159 (MJM) and 141017 (ML), the NOT studentship programme (ML), the Knut and Alice Wallenberg Foundation and the Swedish Research Council (OK), the Väisälä foundation (PK), and the Finnish Graduate School in Astronomy (JL).

## References

Berdyugina, S.V., Tuominen, I.: 1998, A&A 336, L25
Berdyugina, S.V., Jankov, S., Ilyin, I., Tuominen, I., Fekel, F.C.: 1998a, A&A 334, 863
Berdyugina, S.V., Berdyugin, A.V., Ilyin, I., Tuominen, I.: 1998b, A&A 340, 437
Berdyugina, S.V., Berdyugin, A.V., Ilyin, I., Tuominen, I.: 1999, A&A 350, 626
Bopp, B.W., Noah, P.V.: 1980, PASP 92, 333
Carroll, T.A., Kopf, M., Strassmeier, K.G., Ilyin, I., Tuominen, I.: 2009, in: K.G. Strassmeier, A.G. Kosovichev, J. Beckmann (eds.), *Cosmic Magnetic Fields: From Planets, to Stars and Galaxies*, IAU Symp. 259, p. 437
Doyle, J.G., Butler, C.J., Byrne, P.B., et al: 1989, A&A 223, 219

Gustafsson, B., Edvardsson, B., Eriksson, K., et al.: 2008, A&A 486, 951
Hackman, T., Jetsu, L., Tuominen, I.: 2001, A&A 374, 171
Hackman, T., Mantere, M.J., Lindborg, M., et al.: 2011, A&A, submitted, Paper II
Henry, G.W., Eaton, J.A., Hamer, J., Hall, D.S.: 1995, ApJS 97, 513
Ilyin, I.V.: 2000, PhD Thesis, University of Oulu
Jetsu, L., Pelt, J.: 1999, A&AS 139, 629
Jetsu, L., Lehtinen, J., Kajatkari, P., Hackman, T., Henry, G.W.: 2011, A&A, in prep.
Käpylä, P.J., Mantere, M.J., Hackman, T.: 2011, ApJ 742, 34
Kochukhov, O., Piskunov, N., Ilyin, I., Tuominen, I.: 2009, in: K.G. Strassmeier, A.G. Kosovichev, J. Beckmann (eds.), *Cosmic Magnetic Fields: From Planets, to Stars and Galaxies*, IAU Symp. 259, p. 439
Krause, F., Rädler, K.-H.: 1980, *Mean-Field Magnetohydrodynamics and Dynamo Theory*, Pergamon Press, Oxford
Lehtinen, J., Jetsu, L., Hackman, T., Kajatkari, P., Henry, G.: 2011, A&A 527, A136
Lindborg, M., Korpi, M.J., Hackman, T., et al.: 2011, A&A 526, A44, Paper I
Makarov, V.V.: 2003, AJ 126, 1996
Ottmann, R., Pfeiffer, M.J., Gehren, T.: 1998, A&A 338, 661
Piskunov, N.E.: 1991, in: I. Tuominen, D. Moss, G. Rüdiger (eds.), *The Sun and Cool Stars. Activity, Magnetism, Dynamos*, LNP 380, IAU Coll. 130, p. 309
Rodonò, M., Messina, S., Lanza, A.F., Cutispoto, G., Teriaca, L.: 2000, A&A 358, 624
Roettenbacher, R.M., Harmon, R.O., Vutisalchavakul, N., Henry, G.W.: 2011, AJ 141, 138
Rucinski, S.M.: 1977, PASP 89, 280
Siwak, M., Rucinski, S., Matthews, J., et al.: 2010, MNRAS 408, 314
Stoica, P., Selén, Y.: 2004, IEEE Signal Processing Magazine 21, 36
Tuominen, I., Berdyugina, S.V., Korpi, M.J.: 2002, AN 323, 367
Vogt, S.S.: 1979, PASP 91, 616